RADIO MEASUREMENTS OF THE HEIGHT OF STRONG CORONAL MAGNETIC FIELDS ABOVE SUNSPOTS AT THE SOLAR LIMB

JEFFREY W. BROSIUS

Catholic University of America at NASA Goddard Space Flight Center, Code 612.1, Greenbelt, MD 20771; brosius@comstoc.gsfc.nasa.gov

AND

STEPHEN M. WHITE

Department of Astronomy, University of Maryland, College Park, MD 20742; white@astro.umd.edu

ABSTRACT

We measure coronal magnetic field strengths of 1750 G at a height of 8000 km above a large sunspot in NOAA AR 10652 at the west solar limb on 2004 July 29 using coordinated observations with the Very Large Array, the *Transition Region and Coronal Explorer*, and three instruments (CDS, EIT, MDI) aboard the *Solar and Heliospheric Observatory*. This observation is the first time that coronal radio brightness temperatures have been analyzed in a 15 GHz solar radio source projected above the limb. Observations at 8 GHz yield coronal magnetic field strengths of 960 G at a height of 12,000 km. The field strength measurements combine to yield a magnetic scale height $L_B = 6900$ km. The radio brightness temperature maxima are located away from a sunspot plume that appears bright in EUV line emission formed at temperatures around several $\times 10^5$ K. We use the density-sensitive emission-line intensity ratio of O IV 625.8 Å/554.5 Å to derive an electron density n_e (in units of cm^{-3}) of log $n_e = 10.1 \pm 0.2$ at the base of the plume.

Subject headings: Sun: activity — Sun: corona — Sun: magnetic fields — Sun: radio radiation — sunspots — Sun: UV radiation

1. INTRODUCTION

Magnetic fields are widely believed to play a major role in solar coronal physics, from global properties like heating and wind aceleration to energetic transient phenomena like flares and coronal mass ejections. To understand the physical processes that drive these phenomena, therefore, it is essential to have reliable measurements of the magnetic field in the solar corona. However, such measurements are anything but routine. Here we present radio measurements of strong coronal magnetic fields above sunspots at the west solar limb that permit a rare direct determination of the magnetic scale height in the corona.

Two mechanisms can contribute to the radio emission from nonflaring coronal plasma: thermal bremsstrahlung (free-free) and thermal gyroemission (Kundu 1965; Zheleznyakov 1970). Thermal bremsstrahlung is emitted when unbound electrons collide with protons, and its intensity depends on the column emission measure (CEM) and the plasma temperature (e.g., Brosius et al. 1993; Brosius 2004; Gelfreikh 2004). Thermal bremsstrahlung is the minimum possible radio intensity emitted by a plasma. Thermal gyroemission originates from thermal electrons spiraling along coronal magnetic field lines, and its intensity depends on the coronal density, temperature, magnetic field strength, and angle between the magnetic field and the line of sight (e.g., Zlotnik 1968; Holman & Kundu 1985; White & Kundu 1997; Brosius et al. 1997, 2002; White 1999, 2004). Gyroemission occurs when the radio observing frequency (ν) is a harmonic ($n = 1, 2, 3, \ldots$) of the electron gyrofrequency ($\nu_B = B/357$ GHz, where B is the magnetic field strength in units of gauss) in the radio source, so that $B = 357\nu/n$. The direct dependence of gyroemission on the magnetic field strength enables us to use radio observations to derive the magnetic field strength in the solar atmosphere above sunspots.

Unfortunately, observations of radio gyroemission on the solar disk do not directly provide height information about the source; height information must be extracted through assump-

tions and modeling (Brosius 2004; White 2004; Brosius et al. 1997, 2002; Lee et al. 1998, 1999; Vourlidas et al. 1997; Aschwanden & Bastian 1994). This is why we attempted to observe an active region at the solar limb: to unambiguously determine the height dependence of the coronal magnetic field. We were extremely fortunate to have had a pair of large sunspots in our target region at the solar limb during our campaign.

2. OBSERVATIONS AND DATA REDUCTION

We observed NOAA AR 10652 at the west solar limb ($+955''$, $+111''$) with the Coronal Diagnostic Spectrometer (CDS; Harrison et al. 1995) aboard the *Solar and Heliospheric Observatory* (*SOHO*) from 13:32 to 21:41 UT on 2004 July 29 as part of Joint Observing Program (JOP) 100. Coordinated observations with the Very Large Array (VLA) were obtained between 13:30 and 19:30 UT. Full-disk images from *SOHO*'s Extreme-ultraviolet Imaging Telescope (EIT; Delaboudinière et al. 1995) were used to adjust the CDS pointing coordinates, and full-disk white-light images from *SOHO*'s Michelson Doppler Imager (MDI; Scherrer et al. 1995) were used to locate the sunspots near the limb. Photospheric longitudinal magnetograms (from MDI) of the region when it was on the disk reveal that it contained two large spots with positive (outward) magnetic polarity and nearby patches of negative (inward) polarity. Images of the region in white light and at 171, 195, and 1600 Å were also obtained by the *Transition Region and Coronal Explorer* (*TRACE*; Handy et al. 1999). We projected *SOHO* images back to Earth's reference frame (where *TRACE* and the VLA are located) by increasing the pixel sizes of the *SOHO* images by nearly 1%; this compensated for *SOHO* being closer to the Sun than *TRACE* or the VLA.

We used the 4″-wide, 240″-long CDS slit in raster mode to obtain spatially resolved EUV spectra at 60 successive pointings across a $4' \times 4'$ field of view. The CDS spatial resolution was nominally $4''.0 \times 6''.7$. Each scan required 2 hr to complete, so four scans were run during our 8 hr observing period. Here
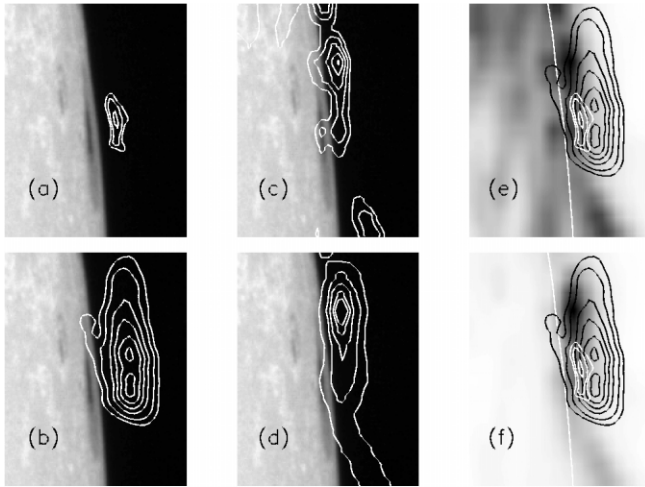
Fig. 1.—Co-aligned white-light (from *TRACE*), EUV (from CDS), and radio (from the VLA) observations of AR 10652 at the west limb on 2004 July 29, all obtained at times close to 18:30 UT as described in the text. Frames *a–d* show white-light images with (*a*) 15 GHz radio intensity contours of 1.5, 3.0, and 6.0 × 10^5 K; (*b*) 8 GHz radio intensity contours of 0.125, 0.25, 0.5, 0.75, 1.0, and 1.25 × 10^6 K; (*c*) O v 629.7 Å intensity contours of 2500, 3000, 3500, 4000, and 4500 ergs cm^{-2} s^{-1} sr^{-1}; and (*d*) Ne vi 562.8 Å intensity contours of 200, 400, 600, 800, and 900 ergs cm^{-2} s^{-1} sr^{-1}. Frame *e* shows the negative intensity image of O v at 629.7 Å, and frame *f* shows the negative intensity image of Ne vi at 562.8 Å, with the same 15 and 8 GHz radio intensity contours displayed in frames *a* and *b*. The limb is drawn as a white contour in frames *e* and *f*. Solar north is up, and west is to the right in this 70″ × 90″ field of view.

we focus on only the scan obtained from 17:37 to 19:39 UT (centered around 18:38 UT). The CDS spectra were processed and calibrated with standard SolarSoftware IDL procedures. We extracted integrated intensity images (60 × 36 arrays) for the emission lines used in this work from the spatially resolved spectra by fitting "broadened Gaussians" (Thompson 1999) to the line profiles in each spatial pixel. Thompson's (1999) procedure accommodates the profile broadening and asymmetry that resulted from the temporary loss of *SOHO* attitude control in 1998; it calculates the profile amplitude A (in units of ergs cm^{-2} s^{-1} sr^{-1} Å^{-1}), centroid wavelength (in angstrom units), and "broadened width" w (effectively the FWHM, in angstrom units). For wavelengths between 513 and 633 Å (all lines in the present work), integrated line intensities (in units of ergs cm^{-2} s^{-1} sr^{-1}) are calculated with $I = 1.485 Aw$. Emission lines used in this work are emitted by ions formed at temperatures ranging from 10^4 to 2 × 10^6 K and include He i, O iii, O iv, O v, Ne iv, Ne v, Ne vi, Ne vii, Ca vii, Ca viii, Ca x, Mg x, Al xi, and Si xii.

We used EIT's full-disk, 2″.63 pixel solar images in He ii 304 Å, Fe ix/x 171 Å, Fe xii 195 Å, and Fe xv 284 Å obtained during our CDS raster scan to improve the CDS co-alignment, which by itself is accurate to only about 15″. Improvement was achieved by visually co-aligning CDS intensity images with the EIT images in emission lines formed at comparable temperatures. The method is described in greater detail by Brosius & White (2004) and Brosius (2005).

Images from *TRACE* offer the highest available spatial resolution of the active region as it approaches the west limb. However, the absolute pointing of *TRACE* is uncertain by as much as 10″. Therefore, in order to co-align the *TRACE* images with our other observations, we co-aligned the *TRACE* white-light images with those from MDI (which are acquired every 96 minutes and show the full disk, so that their pointing in-

formation can be independently confirmed), rotated to match the times of the *TRACE* images exactly. Co-alignments of the sunspots and the limb in the MDI and *TRACE* images were achieved to subpixel accuracy and revealed that the *TRACE* pointing coordinates needed to be shifted by 6″.5 east-west and 1″.5 north-south.

We used the VLA to obtain radio brightness temperature maps at observing frequencies of 14.665 and 8.065 GHz, hereafter referred to simply as 15 and 8 GHz. (Images of the region at 5 GHz were also obtained, but their spatial resolution is poorer than those of the 15 and 8 GHz images, and the uncertainty in the height information is such that they are not useful for this study.) The VLA was in its most compact ("D") configuration, best suited for viewing large, extended structures. The spatial resolution (beam width) of the radio images was 3″ at 15 GHz and 6″ at 8 GHz. The brightness temperature scale was set by standard solar calibration techniques implemented in the VLA receivers. This calibration is reliable to ~20% at 8 GHz where data from many receivers can be compared to determine the correct scale, but at 15 GHz only one receiver could be used on this day, and so the uncertainty approaches 30% in the 15 GHz brightness temperature scale. These uncertainties do not affect the results reported here. To account for the quiet-Sun radio brightness temperature background (Zirin et al. 1991), we added a constant value of 1.14 × 10^4 K to the 15 GHz image and 1.26 × 10^4 K to the 8 GHz image. The absolute pointing of the VLA is well determined, and we confirmed this by comparison of features common to the radio and coronal EUV images. Thus, the radio maps were readily co-aligned with the EIT, CDS, MDI, and *TRACE* data, and the uncertainty in the co-alignment of our observations on July 29 is of order 1″.

Because the VLA's solar amplitude calibration procedure requires that the Sun largely fill the telescope beam, the center of the field of view even for sources near the limb must be located on the solar disk. For the observations reported here, the VLA tracked a location inside the limb during the 6 hr observing period, compensating for rotation of the solar surface at the center of the beam. Thus, the pointing center moved relative to the apparent center of the solar disk during the observation while the solar limb did not move. We separated the VLA data into seven blocks 50 minutes apart (the calibration cycle time) and mapped these blocks independently using the CLEAN algorithm for deconvolution. Each block is composed of five 2 minute scans acquired over a 34 minute period within the 50 minutes (different observing frequencies were alternated in 2 minute scans throughout the observation to obtain the best possible *u-v* coverage). All data are self-calibrated in phase to remove telescope errors and improve the images, and this shifts the data from the individual 2 minute scans as if they were all observed at a common time at the middle of the observing period used. We could clearly see the motion due to solar rotation in the time-dependent sequence of images and account for it carefully in the analysis. Here we focus on only the block whose central time (18:34 UT) most closely matches that of the CDS raster (18:38 UT) used in this work.

3. RESULTS

Figure 1 displays co-aligned white-light, EUV, and radio observations of AR 10652 at the west solar limb around 18:30 UT (see above) on 2004 July 29. The region's large trailing sunspot is clearly visible in white-light emission (frames *a–d*) at the edge of the disk. The 15 GHz source appears

well above the limb and has a peak intensity (radio brightness temperature) of 6.9×10^5 K. The circular polarization of the radio emission is very small at this peak. This observation is the first time that brightness temperatures this large have been observed in a 15 GHz solar radio source above the limb.

We calculated the free-free radio brightness temperature at the location of the 15 GHz intensity peak using the CEM derived from our EUV emission-line intensities. We have assumed the Feldman et al. (1992) coronal elemental abundances (see also Brosius & Landi 2005). The resulting brightness temperature is only 3.4×10^4 K, which indicates that gyroemission must dominate the emission from the 15 GHz source.

White & Kundu (1997) plotted the angular dependence of the optical depths for second, third, and fourth harmonic gyroemission, where the angle is that between the magnetic field and the line of sight (see also Zlotnik's 1968 formulae for gyroresonant opacities). Their calculations show that harmonics greater than the fourth harmonic have no significant optical depth in the quiescent solar corona and that the fourth harmonic is unlikely to be optically thick in both modes of electromagnetic wave propagation (the extraordinary mode and the ordinary mode) simultaneously. This means that fourth harmonic gyroemission would produce a highly polarized source. Since the circular polarization at the peak of the observed 15 GHz source is small, we rule out all harmonics except the second or third for this emission. If the observed 15 GHz source were due to second harmonic gyroemission, it would require a magnetic field strength of 2600 G in the corona. Although we cannot rule this out, such a field strength is larger than photospheric values measured in most sunspots. Furthermore, if a magnetic field strength of 2600 G were present in the corona, it would be surrounded by areas (essentially shells) of successively smaller field strengths since the ambient coronal magnetic field is much weaker than 2600 G. Thus, the path from a second harmonic source at 2600 G would necessarily traverse a third harmonic layer at 1750 G (for our radio observing frequency of 14.665 GHz) on its way to the VLA. Since White & Kundu (1997) have shown that the third harmonic is optically thick to both modes of radio propagation over a wide range of angles, we conclude that third harmonic gyroemission is responsible for our observed 15 GHz radio source. This occurs at a height of about 8000 km above the umbra's center in the sunspot at the limb (see Fig. 1, frame a).

Frame b of Figure 1 shows that there are two peaks in the 8 GHz source above the solar limb, the northern of which has a maximum brightness temperature of 1.3×10^6 K and the southern of which has a maximum brightness temperature of 1.4×10^6 K. This is consistent with our observations of the same region on 2004 July 25 (to be presented in a later publication), when it was on the disk. The calculated free-free radio brightness temperatures at the two 8 GHz peaks are about 6×10^4 K, which indicates that gyroemission dominates their emission. The circular polarization of the radio emission is small at both 8 GHz peaks. A similar argument to that provided above for the 15 GHz source leads us to conclude that third harmonic gyroemission is responsible for our observed 8 GHz radio source. Thus, we find magnetic field strengths of 960 G at heights of about 12,000 km above the umbral center in the sunspot at the limb (see Fig. 1, frame b). Combining the above coronal magnetic field strengths that correspond to third harmonic gyroemission at our two radio observing frequencies with the observed separations of the radio source peaks, we derive a magnetic scale height $L_B = B/\nabla B$ of 6.9×10^3 km.

Frames c and d of Figure 1 show EUV intensity contours

of the O v emission line at 629.7 Å and the Ne vi emission line at 562.8 Å. These lines are formed at temperatures around 2.5×10^5 K (log $T = 5.4$) and 4.0×10^5 K (log $T = 5.6$), respectively, where sunspot plumes generally appear very bright (Foukal et al. 1974; Foukal 1976; Fludra et al. 1997; Maltby et al. 1998; Brynildsen et al. 2001; Brosius & White 2004; Brosius 2005; Brosius & Landi 2005). The bright EUV source in the northern half of frames c and d corresponds to sunspot plume emission. As is the case in this sunspot, plume emission is frequently located above a spot's penumbra but is not necessarily located above the umbra. The extended structure outlined by only one EUV contour in the southern half of frame d is the leg of a transequatorial loop connected to NOAA AR 10653 in the southern hemisphere (Brosius 2006).

Frames e and f display EUV negative intensity images along with 8 and 15 GHz intensity contours. These show that the largest radio intensities are located away from the brightest EUV (sunspot plume) emission. At the O v and Ne vi EUV intensity peaks, we find that the observed 8 GHz intensities exceed their calculated free-free values by factors of 3.0 and 4.7, respectively, which indicates that the observed 8 GHz emission from the EUV plume is dominated by thermal gyroemission. This is consistent with Brosius & White (2004), who obtained coordinated observations of the large sunspot in NOAA AR 8539 (near disk center) on 1999 May 9 and 13 with *SOHO* and the VLA. They demonstrated that the radio emission from the sunspot umbra was dominated by thermal gyroemission from the plume, which accounted for radio brightness temperatures $<1 \times 10^6$ K in the umbra on both dates, as well as a distinct depression in the umbra's radio brightness temperature on May 13. We find that the observed 15 GHz intensities at the O v and Ne vi EUV intensity peaks are actually smaller than their calculated free-free values, most likely due to noise in the weak 15 GHz emission far from the source peak.

We used the density-sensitive intensity ratio of the O iv lines at 625.8 and 554.5 Å to derive the electron density in an $8'' \times 13''$ area at the base of the sunspot plume. This is the most reliable density-sensitive ratio available to us. Since all four components of the O iv multiplet around 554.5 Å are blended in our observations, we included all of them in the theoretical density sensitivity curve derived from the CHIANTI (ver. 4) database (Dere et al. 1997; Young et al. 2003). The measured intensities at 625.8 and 554.5 Å are, respectively, 10.8 ± 2.2 and 1720 ± 340 ergs cm^{-2} s^{-1} sr^{-1}, where the (20%) uncertainties account for uncertainties in both the CDS calibration and the theoretical atomic physics parameters. The intensity ratio is 0.00625 ± 0.00177, from which we derive log $n_e = 10.1 \pm 0.2$. This is greater than the values of $9.6^{+0.3}_{-0.6}$ and $9.7^{+0.2}_{-0.2}$ reported by Brosius & Landi (2005) using the same O iv ratio for the sunspot plume observed on 1999 May 9 and 13, but the difference may not be significant in light of the uncertainties.

4. DISCUSSION AND CONCLUSIONS

We were fortunate to have had a large sunspot at the solar limb during our observing campaign. This enabled us to use radio gyroemission to directly, accurately, unambiguously measure the height dependence of the coronal magnetic field. From these measurements, we derived a magnetic scale height $L_B = 0.69 \times 10^9$ cm, which agrees remarkably well with values presented by previous authors. For example, Gary et al. (1993) used sunspot observations with the Owens Valley Radio

Observatory (OVRO) during a solar eclipse to obtain a lower bound on L_B of 0.73 × 10^9 cm. Lee et al. (1993) used the solar limb occultation of a sunspot radio source observed with OVRO to estimate $L_B \sim 0.54 \times 10^9$ cm. Kruger et al. (1986) used RATAN-600 sunspot radio observations to obtain an average value for L_B of (0.74 ± 0.23) × 10^9 cm. Aschwanden et al. (1995) obtained (2.4 ± 0.1) × 10^9 cm from stereoscopic altitude measurements of the main peak of a sunspot's radio brightness distribution obtained with OVRO on 4 successive days.

One possible anomaly in the radio observations reported here is that coronal brightness temperatures in the gyroresonance sources do not extend down to the base of the corona, which is reported to be at heights of about 2500 km (Auchere et al. 1998; Zhang et al. 1998). The most likely reason for this is absorption at radio wavelengths by cool material (such as spicules extending up from the chromosphere) in these lower heights. Other observations of the quiet solar disk at radio wavelengths show that the radio limb can appear 8000 km or more above the photosphere (Hanaoka et al. 1994; Gary 1996). Absorption by cool material in the low corona would not affect our determination of the magnetic scale height, since our derivation of L_B requires only that the tops of the gyroresonance sources be visible above any absorption layers.

The Alfvén speed V_A (in units of cm s^{-1}) is given by $B/(4\pi\rho)^{1/2}$, where B is in units of gauss and ρ is the mass density in units of gm cm^{-3}. This is the speed at which transverse waves propagate along magnetic field lines, thus characterizing a means by which wave energy can be transported from one location in the solar atmosphere to another, possibly providing some of the energy required to heat the corona or drive the solar wind. We calculate V_A of 34,000 and 19,000 km s^{-1} at the 15 and 8 GHz radio brightness temperature maxima, respectively, assuming that our measured electron density at the base of the plume is valid there. Since the coronal density is likely to be smaller than this, the above values are actually lower limits. Assuming a coronal electron density of 4 × 10^9 cm^{-3}, we derive corresponding speeds of 60,000 and 33,000 km s^{-1}. These speeds are comparable to those derived by Brosius et al. (2002) in the 1 × 10^6 K plasma above a large sunspot observed on the disk.

To summarize, we measure a coronal magnetic field strength of 1750 G at a height of 8000 km above a large sunspot in AR 10652 at the west solar limb on 2004 July 29 using coordinated observations with the VLA, *TRACE*, and three instruments (CDS, EIT, MDI) aboard *SOHO*. This observation is the first time that coronal radio brightness temperatures (6.9 × 10^5 K) have been analyzed in a 15 GHz solar radio source projected above the limb. Observations at 8 GHz yield coronal magnetic field strengths of 960 G at a height of 12,000 km. Both the 15 and 8 GHz sources are unpolarized at their respective peaks. The field strength measurements combine to yield a magnetic scale height L_B = 6900 km.

REFERENCES

Aschwanden, M. J., & Bastian, T. S. 1994, ApJ, 426, 425
Aschwanden, M. J., Lim, J., Gary, D. E., & Klimchuk, J. A. 1995, ApJ, 454, 512
Auchere, F., Boulade, S., Koutchmy, S., Smartt, R. N., Delaboudiniere, J. P., Georgakilas, A., Gurman, J. B., & Artzner, G. E. 1998, A&A, 336, L57
Brosius, J. W. 2004, in Solar and Space Weather Radiophysics, ed. D. E. Gary & C. O. Keller (Dordrecht: Kluwer), 265
———. 2005, ApJ, 622, 1216
———. 2006, ApJ, 636, L57
Brosius, J. W., Davila, J. M., Thomas, R. J., & White, S. M. 1997, ApJ, 488, 488
Brosius, J. W., & Landi, E. 2005, ApJ, 632, 1196
Brosius, J. W., Landi, E., Cook, J. W., Newmark, J. S., Gopalswamy, N., & Lara, A. 2002, ApJ, 574, 453
Brosius, J. W., & White, S. M. 2004, ApJ, 601, 546
Brosius, J. W., et al. 1993, ApJ, 411, 410
Brynildsen, N., Maltby, P., Fredvik, T., Kjeldseth-Moe, O., & Wilhelm, K. 2001, Sol. Phys., 198, 89
Delaboudinière, J.-P., et al. 1995, Sol. Phys., 162, 291
Dere, K. P., Landi, E., Mason, H. E., Monsignori-Fossi, B. C., & Young, P. R. 1997, A&AS, 125, 149
Feldman, U., Mandelbaum, P., Seely, J. L., Doschek, G. A., & Gursky, H. 1992, ApJS, 81, 387
Fludra, A., Brekke, P., Harrison, R. A., Mason, H. E., Pike, C. D., Thompson, W. T., & Young, P. R. 1997, Sol. Phys., 175, 487
Foukal, P. V. 1976, ApJ, 210, 575
Foukal, P. V., Huber, M. C. E., Noyes, R. W., Reeves, E. M., Schmahl, E. J., Timothy, J. G., Vernazza, J. G., & Withbroe, G. L. 1974, ApJ, 193, L143
Gary, D. E. 1996, in ASP Conf. Ser. 93, Radio Emission from the Stars and the Sun, ed. A. R. Taylor & J. M. Paredes (San Francisco: ASP), 387
Gary, D. E., LeBlanc, Y., Dulk, G. A., & Golub, L. 1993, ApJ, 412, 421
Gelfreikh, G. B. 2004, in Solar and Space Weather Radiophysics, ed. D. E. Gary & C. O. Keller (Dordrecht: Kluwer), 115

Hanaoka, Y., et al. 1994, in Proc. Kofu Symp., New Look at the Sun with Emphasis on Advanced Observations of Coronal Dynamics and Flares, ed. S. Enome & T. Hirayama (Nagano: NAOJ), 35
Handy, B. N., et al. 1999, Sol. Phys., 187, 229
Harrison, R. A., et al. 1995, Sol. Phys., 162, 233
Holman, G. D., & Kundu, M. R. 1985, ApJ, 292, 291
Kruger, A., Hildebrandt, J., Bogod, V. M., Korzhavin, A. N., Akhmedov, S. B., & Gelfreikh, G. B. 1986, Sol. Phys., 105, 111
Kundu, M. R. 1965, Solar Radio Astronomy (New York: Wiley)
Lee, J., Gary, D. E., & Hurford, G. J. 1993, Sol. Phys., 144, 349
Lee, J., McClymont, A. N., Mikic, Z., White, S. M., & Kundu, M. R. 1998, ApJ, 501, 853
Lee, J., White, S. M., Kundu, M. R., McClymont, A. N., & Mikic, Z. 1999, ApJ, 510, 413
Maltby, P., Brynildsen, N., Brekke, P., Haugan, S. V. H., Kjeldseth-Moe, O., & Wikstol, O. 1998, ApJ, 496, L117
Scherrer, P. H., et al. 1995, Sol. Phys., 162, 129
Thompson, W. T. 1999, CDS Software Note 53 (Greenbelt: NASA/GSFC), http://solar.bnsc.rl.ac.uk/software/notes.shtml
Vourlidas, A., Bastian, T. S., & Aschwanden, M. J. 1997, ApJ, 489, 403
White, S. M. 1999, Sol. Phys., 190, 309
———. 2004, in Solar and Space Weather Radiophysics, ed. D. E. Gary & C. O. Keller (Dordrecht: Kluwer), 89
White, S. M., & Kundu, M. R. 1997, Sol. Phys., 174, 31
Young, P. R., Del Zanna, G., Landi, E., Dere, K. P., Mason, H. E., & Landini, M. 2003, ApJS, 144, 135
Zhang, J., White, S. M., & Kundu, M. R. 1998, ApJ, 504, L127
Zheleznyakov, V. V. 1970, Radio Emission of the Sun and Planets, ed. J. S. Hey (Oxford: Pergamon)
Zirin, H., Baumert, B. M., & Hurford, G. J. 1991, ApJ, 370, 779
Zlotnik, E. Y. 1968, Soviet Astron., 12, 245